

**Development and Application of  
Laser-Induced Incandescence (LII)  
as a Diagnostic for  
Soot Particulate Measurements**

David R. Snelling, Gregory J. Smallwood,  
Ian G. Campbell, Jennifer E. Medlock, and Ömer L. Gülder

National Research Council Canada  
Ottawa, Ontario, Canada  
K1A 0R6

presented at:

AGARD 90<sup>th</sup> Symposium of the Propulsion and Energetics Panel on  
Advanced Non-Intrusive Instrumentation for Propulsion Engines

20-24 October 1997, Brussels, Belgium

# Development and application of laser induced incandescence (LII) as a diagnostic for soot particulate measurements

D. R. Snelling, G. J. Smallwood, I. G. Campbell, J. E. Medlock and Ö. L. Gülder

National Research Council of Canada

Building M-9, Montreal Road

Ottawa, ON, Canada K1A 0R6

## 1. SUMMARY

LII is a promising diagnostic for *in-situ* measurements of particulates. The LII signal is shown to be proportional to soot volume fraction. Due to the large dynamic range of the LII technique, we have been able to measure time-averaged soot concentrations in the part per billion range with a spatial resolution of ~0.5 mm in each dimension. The decay of the LII signal in the post evaporative region is shown to be a sensitive measure of primary particle size. A numerical model has been developed which accurately predicts post evaporative LII signal decay rates. The prediction of the excitation curve is unsatisfactory, with more work needed to correctly model the particle behaviour during the soot evaporation phase.

Also, the model predicts that the prompt LII signal will vary as the 3.33 power of particle diameter. However, this predicted departure from strict proportionality between LII signal and soot volume fraction was not experimentally observed.

## 2. INTRODUCTION

Soot volume fraction measurements are important for studies of soot formation, radiation processes, and for monitoring post-flame particulates. Light extinction is a commonly used diagnostic technique for measuring soot volume fraction. However, it suffers from the drawback of measuring a line-of-sight average, and while tomographic reconstruction can be used to calculate soot profiles in radially symmetric flames, this is not possible in turbulent flames. Elastic scattering of light has been widely investigated for soot measurements but the fact that the signal is proportional to the square of the particle diameter means that the technique is more useful for particle sizing than volume fraction measurements. More importantly, for agglomerated soot particles (which are definitely not spherical), it has become increasingly clear in the last few years that the approach of applying Mie theory by assuming spherical soot particles results in large errors<sup>1-4</sup>.

Laser induced incandescence (LII) has emerged as a promising technique for measuring spatially and temporally resolved soot volume fraction in flames<sup>5-14</sup>. In LII the soot is heated by a short duration laser pulse to produce incandescence. With sufficiently high laser energies, numerical models of the heat transfer indicate

that the soot particles reach temperatures of 4000-4500 K.<sup>5,6,10,12,13</sup> The resultant radiation, which is blue shifted relative to soot radiation at normal flame temperatures and is of short duration, can readily be detected. LII typically has a temporal resolution of 10 ns and can be used to perform both point measurements and 2-D planar visualization.

In this paper we describe our development of the LII technique for point measurement in flames. Since LII provides only relative soot volume fraction measurements, an absolute calibration is necessary. This was performed in a simple laminar diffusion flame, where the radial soot volume fraction profiles were measured by Abel inversion of line-of-sight attenuation measurements. We have implemented a numerical model of the LII processes to aid in the interpretation of experimental results. Model predictions and their comparison to experiment are presented. Finally, the application of LII to a confined C<sub>3</sub>H<sub>8</sub>/air turbulent diffusion flame is investigated.

## 3. EXPERIMENTAL

### 3.1 Laser Induced Incandescence

The schematic of the LII setup is shown in Fig. 1. A Continuum Surelite1 Nd:YAG laser with Gaussian optics operating at its fundamental wavelength of 1064 nm was used as the pulsed light source. The beam quality was improved by inserting an aperture in the laser cavity. This modification reduced the maximum energy to 40 mJ. Further attenuation of the beam, by using a half wave plate to rotate the plane of polarisation in combination with a vertical polariser, was used to control the energy delivered to the flame. The aperture resulted in a laser beam whose near-field intensity distribution was Gaussian.

The beam was then focussed through a beam expander and a cylindrical lens to form a sheet with Gaussian fit parameters ( $1/e^2$  full width) of 3.62 mm (height) and 0.44 mm (width). The beam intensity profiles were near perfect fits to a Gaussian distribution as measured with a Coherent BeamView system. The LII signal from the centre of the laser sheet was imaged at 2:1 magnification with a 54 mm diameter lens of 190 mm focal length onto apertures of 1.06 mm diameter in front of the photomultipliers (PM's). Thus the sample

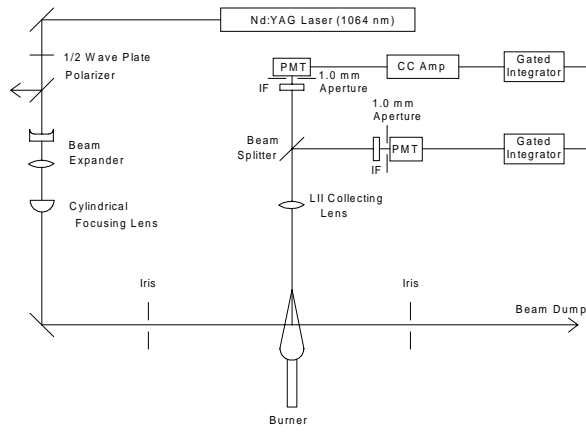


Figure 1 Top-view schematic of LII apparatus.

volume in the flame was a cylinder of diameter 0.53 mm whose length was the width of the laser sheet (0.44 mm).

The LII signal was split equally between two PM's each equipped with an interference filter centred at 455.5 nm with a bandwidth of 11.0 nm. One of the PM's was connected directly to a gated integrator whose gate width was set at 25 ns to measure the peak of the LII signal (subsequently referred to as the prompt signal). The other PM was connected to a charge-coupled amplifier which measured the total charge collected during the LII pulse and thus measured the time integrated LII signal.

### 3.2 Calibration

#### 3.2.1 Flame

The laminar diffusion flame used in these experiments was similar to that used by Gülder<sup>15</sup> except that the fuel tube was 13.9 mm in diameter. The  $C_2H_4$  flow rate was  $3.27 \text{ cm}^3/\text{s}$  and the surrounding air flow rate 170 SLPM. The visible flame height was 67 mm.

#### 3.2.2 Line-of-Sight Attenuation

Both 532 and 1064 nm laser attenuation experiments were performed, with a 3 times beam expander followed by a 1 m focal length lens used to reduce the beam diameter through the flame. At 1064 nm the focal beam diameter in the flame,  $\omega_0$ , was 0.24 mm (Gaussian  $1/e^2$  diameter); and the confocal parameter (total distance between the points at which the beam diameter had increased to  $\sqrt{2} \cdot \omega_0$ ) is 160 mm. This ensured that there was little variation in beam size across the maximum flame diameter, which was 6 mm at the heights investigated.

A beam splitter directed part of the pre-flame laser beam onto a silicon photodiode detector (detector A) and the transmitted laser beam was measured with a second detector (B). Signals from both detectors were detected with gated integrators whose outputs were

ratioed to give A/B on a shot-by-shot basis. In this way we were able to correct for small changes in laser pulse energy, and the flame transmission could be measured to an accuracy of  $\sim 0.25\%$ . The transmission measurements were made every 0.1 mm across the flame, at heights of 30, 35, and 40 mm.

## 4. RESULTS AND ANALYSIS

### 4.1 Attenuation Results

In the Rayleigh limit the soot volume fraction,  $f_v$ , is given by

$$f_v = \frac{\ln(T) \lambda}{6 \pi L E(m)} \quad (1)$$

where T is the flame transmission,  $\lambda$  the wavelength and L the flame width. The complex refractive index is denoted by  $m=n+ik$ , and  $E(m) = -\text{Im}\{(m^2 - 1)/(m^2 + 2)\}$ , thus

$$E(m) = \frac{6nk}{(n^2 - k^2 + 2)^2 + 4n^2k^2} \quad (2)$$

Using the dispersion relationship from Dalzell and Sarofim<sup>16</sup> to calculate the refractive index we obtain:  $m=1.59+0.58i$  and  $E(m)=0.264$  at 532 nm; and  $m=1.63 + 0.7i$  and  $E(m)=0.303$  at 1064 nm.

The Abel inversion of the transmission measurements was performed using the 3 point Abel algorithm of Dasch<sup>17</sup> with a data spacing at the recommended 0.2 mm. The resultant curves are shown in Fig.2, where it can be seen that there is generally very good agreement between the 532 nm and 1064 nm data. This agreement is not necessarily expected since the undesirable effect of scattering is enhanced with decreasing wavelength, increasing the laser attenuation beyond what would be expected from absorption, and can thus lead to an

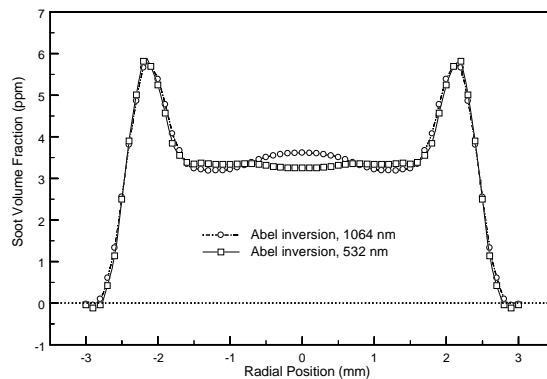


Figure 2 Comparison of radial profiles from Abel inversion of line-of-sight attenuation data acquired at 532 nm and 1064 nm. Data was acquired at a height of 40 mm in an ethylene/air flame.

overestimate of the soot concentration.<sup>2,18,19</sup> For visible wavelengths, errors of 30-100% in soot concentration are expected depending on the size and morphology of the soot agglomerates. The uncertainty in the refractive index and its wavelength dependence can mask such effects.

## 4.2 LII Calibration

LII measurements were performed at the same locations in the laminar diffusion flame. As the energy of the 1064 nm laser is increased (above the LII detection threshold) there is an initial sharp increase in LII signal. With a peak laser fluence (at the centre of the sheet) of 0.32 J/cm<sup>2</sup> a further increase in energy produces very little increase in LII signal as shown in Fig. 3. The LII detection is typically operated in this plateau region.<sup>5,8,13,20,21</sup> We have used a peak laser fluence of 0.48 J/cm<sup>2</sup> for our LII measurements, which are shown in Fig. 4 with the 532 nm Abel inverted data for comparison.

In Fig. 4 the LII data has been scaled to the Abel data so that the integrated soot volume fraction over the total flame width is the same for all the curves. In general it can be seen that there is good agreement between the soot profiles from LII and Abel inverted transmission measurements, with the prompt LII data following the Abel inverted data more closely. Thus in the soot concentration range 0.5-5.0 ppm the prompt LII and the extinction measurements are linearly related. This result is in agreement with other studies that have found a linear relationship over this concentration range.<sup>8,21,22</sup> Vander Wal, using gravimetric sampling for calibration, has observed good linearity in the 0.035-1.5 ppm soot concentration range.<sup>23</sup>

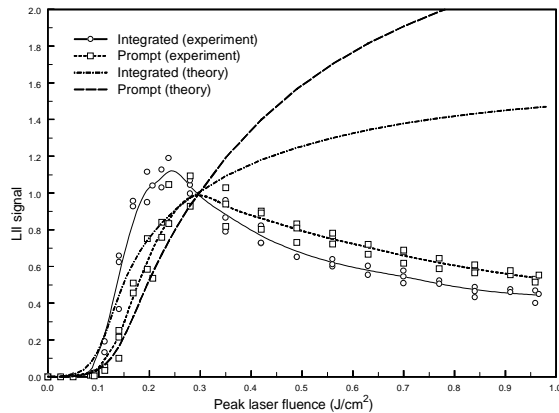


Figure 3 Excitation curves indicating relative LII signal as a function of the peak laser fluence for both prompt and integrated signal detection. Measured and predicted values are shown for the region of maximum soot concentration ( $r = 2.1$  mm) at a height of 40 mm in an ethylene/air flame.

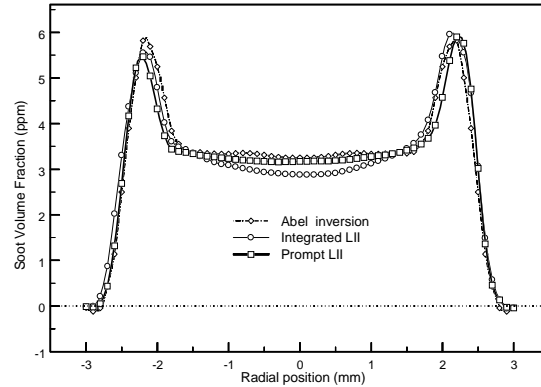


Figure 4 Comparison of soot volume fraction determined by LII to radial profiles from Abel inversion of line-of-sight attenuation data at 40 mm above the burner.

## 5. NUMERICAL MODEL

### 5.1 Heat Transfer To and From Soot Particles

The numerical modelling of the transient heating and subsequent radiation and cooling of soot particles exposed to short duration (10 nsec) laser pulses is briefly described below. The approach is similar to that used by several authors.<sup>6,10,12,13,24,25</sup> Our approach most closely follows that of Hofeldt<sup>10</sup> and only the differences between the two models will be emphasized.

The previous LII numerical modeling has assumed the particles to be equivalent spheres and calculated the absorption from Mie theory.<sup>5,6,10,13</sup> In recent years it has become clear that Mie theory based on equivalent spheres introduces large errors in calculating the scattering and absorption of real soot particles<sup>1-4</sup> (and references contained therein), and that soot absorption is well described by Rayleigh theory, provided that the primary particle diameter is within the Rayleigh limit (significantly smaller than the light wavelength).

The equations describing the soot heat transfer presented here are for a more realistic soot morphology in that we assume the soot particles to be agglomerates of  $N_p$  just touching primary particles of diameter  $d_p$ .<sup>1</sup> This approach has also been recently adopted by Mewes et al.<sup>12</sup>

The heat transfer energy balance equation is:

$$C_a q - \frac{2 K_a (T - T_0) \pi N_p d_p^2}{(D_{ES} + G \lambda_{MFP})} + \frac{H_v}{M_v} \frac{dM}{dt} + q_{rad} - \frac{1}{6} \pi N_p d_p^3 \rho_s c_s \frac{dT}{dt} = 0 \quad (3)$$

The first term,  $C_a q$ , is the absorbed laser energy, where, in the Rayleigh limit, the absorption cross section  $C_a$  is

given by:

$$C_a = \frac{\pi^2 N_p d_p^3 E(m)}{\lambda} \quad (4)$$

This will certainly be true in our experiments since we are clearly in the Rayleigh limit, having used 1064 nm laser excitation.

The second term involves heat transfer to the surrounding medium for a particle in the transition regime between continuum and free molecule (Knudsen) heat transfer. Since the mean free path in the gas is typically much larger than the soot particle diameter, the particle is largely in the free molecule limit, and thus the heat transfer coefficient is independent of particle size.  $G$  is a geometry dependent heat transfer factor<sup>26</sup>, equal to  $8f/(\alpha(\gamma+1))$  where  $f$  is the Eucken factor (5/2 for monatomic species),  $\alpha$  is the accommodation coefficient, and  $\gamma=c_p/c_v$  ( $=1.40$  for air). A value of  $\alpha \sim 0.9$  has generally been adopted in previous work.<sup>6,10,13</sup>

The third term is heat loss due to evaporation of the soot and is given by:

$$\begin{aligned} \frac{dM}{dt} &= \frac{\rho_s}{2} \pi D^2 \frac{dD}{dt} \\ &= -\pi N_p d_p^2 \frac{\frac{P_s(T) N_{AV}}{RT}}{\frac{1}{\beta} \left( \frac{2\pi M_v(T)}{RT_s} \right)^{1/2} + \frac{D_{ES}}{2D_{AB}}} \end{aligned} \quad (5)$$

Again the flux of carbon vapour is dominated by the free molecule regime (the first term in the denominator of Eq. 5) and is independent of particle size. The soot vapour pressure has generally been calculated using fixed values of the heat of vaporisation  $H_v$  and soot vapour molecular weight  $M_v$ . We have used the temperature dependent values of these quantities  $P_s(T)$ ,  $M_v(T)$  calculated using the empirical relationships of Leider et al.<sup>27</sup> in solving the equations.

The fourth term, representing radiative loss for a single primary particle, can be approximated as:

$$q_{rad,p} = 4\pi^2 N_p d_p^3 \sigma_{SB} T^4 \left( \frac{E(m)}{\lambda} \right)_{600} \quad (6)$$

where the expression in parentheses is evaluated at some average wavelength, 600 nm in this case. This approximation, including the selection of evaluation wavelength, is not limiting since soot particle heat loss due to radiation is insignificant compared to the other heat loss terms.

The particle equivalent sphere diameter dependence ( $D_{ES}$ ) in the denominator of Eqs. 3 and 5 is the equivalent sphere diameter given by  $D_{ES}^3 = N_p d_p^3$  and it reflects the dependence of heat transfer and the flux of

evaporating soot on this soot size in the continuum limit. Since the soot particle diameter is very much less than the gas mean free path these continuum terms are not important and for soot evaporation have been neglected in much of the earlier modelling.<sup>6,13</sup> In our approach, these equations constitute a coupled set of differential equations for  $D$  and  $T$  that have been solved numerically using a Runge-Kutta integration routine. From this solution we can calculate the time history of the LII signal using the relationship:

$$I(\lambda) = \frac{2\pi c^2 h}{\lambda^5} \left[ e^{-\frac{hc}{k\lambda T}} - 1 \right]^{-1} \pi N_p d_p^2 K_{ap}(\lambda) d\lambda \quad (7)$$

$$\text{where } K_{ap} = \frac{4\pi d_p E(m)}{\lambda}$$

The LII signal  $I$  is a function of  $T$ ,  $d_p$ ,  $N_p$ , time ( $t$ ), and laser fluence ( $F$ ). To calculate values of  $I$  to compare with experiment we must integrate  $I$  over the range of laser fluence values encountered in the laser sheet. Since our probe volume only occupies a region of the sheet 0.53 mm diameter the distribution of laser fluence is essentially constant in the plane of the sheet. However, there is a Gaussian distribution of fluence across the thickness of the sheet (i.e. along the LII viewing axis). This can be described by

$$F(x) = F_0 \exp\left(-\frac{x^2}{w_x^2}\right) \quad (8)$$

where the sheet half width  $w_x = 0.22$  mm, and  $F_0$  is the peak fluence at the centre of the sheet.  $I(F,t)$  can then be integrated across these fluence values to give a signal  $I_G(t)$  that can be compared to our experiments. The prompt and integrated LII signal for a given laser fluence can be obtained by the appropriate time integration of  $I_G(t)$ .

## 5.2 Comparison Of Model To Experiments

### 5.2.1 LII Excitation

To compare our experimental results to the predictions of the numerical model we need information on both the primary particle diameter and the agglomerate size in our burner. Megaridis and Dobbins<sup>28</sup> have used thermophoretic sampling of an  $C_2H_4$ /air flame, coupled with electron microscopy, to measure the soot primary particle size in the regions of maximum soot concentration. Their burner is very similar to ours but because of small differences in flow rate and burner diameter our flame height (67.5 mm) lower than theirs (88 mm). We have scaled their measurements accordingly to our flame heights to obtain the values shown in Table 1.

We have used the method of solution outline above to calculate the expected dependence of the prompt and integrated LII signal as a function of laser energy. The

Table 1 Primary particle size ( $d_p$ ), number of primary particles per agglomerate ( $N_p$ ), and the equivalent sphere diameter ( $D_{ES}$ ).<sup>28</sup>

Height (mm)	$d_p$ (nm)	$N_p$ (nm)	$D_{ES}$ (nm)
20	13	8	26
30	29.5	35	96.5
35	32	45	113.8
40	32.5	60	127.2

theoretical curves are shown in Fig. 3 where the predicted LII signals are shown as a function of peak laser fluence. Since the LII signal is in arbitrary units, the experimental and theoretical curves have been scaled to a value of 1 at a peak fluence of  $0.3 \text{ J/cm}^2$ .

Although the model satisfactorily predicts the onset of the sharp rise in LII signal, it does not predict the observed fall-off at higher fluence values. The shapes of the experimental excitation curves reported in the literature vary widely. With the exception of Ni et al.<sup>21</sup>, in no other study has the excitation fluence been directly measured and reported. Ni et al.<sup>21</sup> used an aperture close to the flame to ensure constant fluence. They observed an LII signal (measured with an 18 ns gate) that peaked at  $0.35 \text{ J/cm}^2$  and decreased a factor of 2 with a further twofold increase in fluence. Vander Wal et al.<sup>8</sup> observed a similar qualitative behaviour with an imaging system that largely limited the effective fluence variation to that of a presumably Gaussian distribution along the LII collection axis. Other workers<sup>20,22,29</sup> have generally observed a monotonically increasing LII signal with an abrupt decrease in slope at higher fluences.

Our experiences in setting up our experiment was that it was quite difficult to obtain a simple Gaussian distribution of intensities in the LII excitation region. Laser beams whose intensity profiles were markedly non-Gaussian in the near field produced focal images with an intense central spot surrounded by more diffuse, weaker wings. This was particularly true if screens or hard apertures were used to control the laser beam intensity profile. With this type of excitation one would expect an excitation curve that does not saturate since, with increasing laser energy, the weaker radiation in the wings will continue to produce large increases in LII signal after the intense centre core saturates. This points to the necessity of carefully measuring the laser fluence in the region of LII excitation if one is to compare LII saturation behaviour.

The failure of the LII model to successfully predict the saturation at high fluences is quite dramatic and remains to be explained. It should be remembered that the equations describing the evaporation of soot are

only correct in the limit of low vaporization rates<sup>10</sup> which may not be true at the largest excitation fluences used in this and other experiments.

### 5.2.2 LII Decay

It is interesting to compare the experimental LII time decays with model predictions. The experimental decays measured at various radial positions at a 40 mm height in our burner are shown in Fig. 5. The decay curves are, to a good approximation, logarithmic in the time range 300 to 1000 ns. The time constant of these decays decreases dramatically as we go from the region of maximum soot to the centre of the burner. The results of the numeric modelling show that the decay of LII signal in this time range is almost totally dominated by heat transfer to the surrounding gas. Evaporation of soot has ceased to be important with the large drop in particle temperature and radiation is unimportant in this time range. Thus the faster decays are expected since elastic scattering experiments have shown a large decrease in soot particle diameter between the flame centreline and the region of maximum soot.

Using the data in Table 1 we have calculated theoretical decay curves for the region of maximum soot and for the Gaussian excitation used in our experiments. The theoretical curves are shown in Fig. 5 for values of the accommodation coefficient of 0.26 and 0.9. The 0.9 accommodation coefficient curve incorrectly predicts a very fast decay whilst the 0.26 accommodation coefficient curve is in quite good agreement with experiment. The value of 0.9 has been widely used in the literature<sup>6,10,13,14</sup> but recent measurements of the accommodation coefficient of nitrogen on solid graphite in the temperature range 300-1000 K give the value of 0.26<sup>30</sup>. Interestingly, a similar calculation assuming an equivalent sphere diameter for the particle and an accommodation coefficient of 0.9 also give good agreement with experiment. This results from a cancellation of errors in that the equivalent sphere

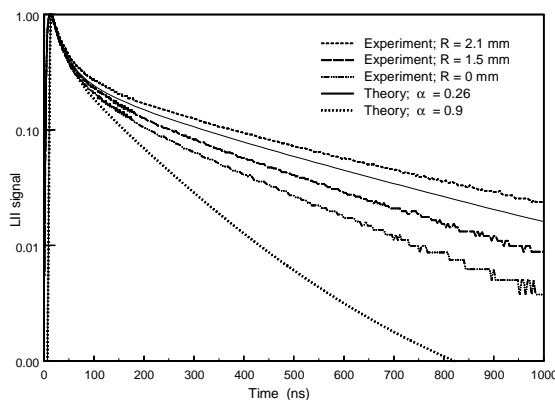


Figure 5 LII signal decay curves indicating variation in time constant in post evaporation ( $>300 \text{ ns}$ ) region. Measured and predicted values are shown for a height of 40 mm in an ethylene/air flame.

model under predicts the heat transfer rate by almost a factor of 4 compared to the agglomerate model, but this is compensated for by the almost 4 times increase in accommodation coefficient.

Will et al.<sup>14</sup> have used LII imaging and ratioed images of LII signals taken at different times to obtain 2-D maps of particle size. The particle size estimation was based on a comparison of the measured decay rate with that calculated from numerical modelling of the soot cooling assuming the particles to be single spheres. It is apparent from our modeling that the size determined from these decays is much closer to that of the primary particle size rather than some average agglomerate size. This conclusion is also supported by the recent analysis of Mewes et al.<sup>12</sup>

We can use our decay data to estimate the primary particle size at the burner centreline. At a height of 40 mm, the ratio of the time constant at  $r=0$  mm (230 ns) to that in the region of maximum soot at  $r=2.1$  mm (375 ns) is 0.61. Since the decay is dominated by heat transfer to the medium, where the heat loss scales as primary particle area,

$$\frac{d_{p_2}^2}{d_{p_1}^2} = \frac{\tau_2}{\tau_1} \quad (9)$$

where  $\tau$  is the LII signal decay time constant. This result implies a primary particle size of 25.5 nm ( $0.61^{1/2} \times 32.5$  nm) at burner centre.

## 6. APPLICATION

To demonstrate the feasibility of eventually applying LII in a gas turbine combustor, preliminary experiments were made in a confined bluff-body stabilized turbulent diffusion flame. This burner was fuelled by propane burning in air at an overall equivalence ratio of 0.65. The flame was stabilized by a weak recirculation zone attached to the bluff-body, and reached a mean peak temperature of 1980 K (Pt/Pt-Rh thermocouple type S) along the centreline of the 100 mm diameter, 400 mm long chamber. The steel walls of the burner were blanketed by insulation to minimize heat transfer losses. A clever window design allowed LII measurements to be made in a grid pattern over an axial range of 57 to 370 mm, at approximately 25 mm steps, and radially at each axial station in 5 mm increments. A weak nitrogen purge minimized soot buildup on the windows.

The incident beam (1064 nm) was unattenuated while the scattered light signal detected at 440 nm suffered attenuation up to 40% in heavy sooting regions. At each grid location 5000 samples of prompt and integrated signals were collected. The mean of the soot volume fractions recorded at each location is reported, providing a time-averaged result in this turbulent flame. Soot was observed to first form at the outer tip of the

recirculation zone, approximately 100 mm from the nozzle. Downstream of the 100 mm point the soot levels increased with axial distance along the centreline and the width of the sooting zone also increased with axial distance, as shown in Fig 6. The highest level of soot, averaging 4 ppb, was located on the centreline at the furthest axial location. From gas chromatography measurements, it is known that the bulk of the fuel and lighter hydrocarbon remained within the "recirculation" zone. However, some fuel penetrated the recirculation zone, to form soot in the slow moving high temperature zone.

Over the measuring region a maximum of only 4% of the 5000 samples produced a measurable LII signal. The probability of a single shot recording a signal significant enough to determine soot volume fraction is indicated in Fig. 7. Unlike the soot volume fraction measurements, this probability did not increase beyond 200 mm from the nozzle, although the width of the zone was observed to expand.

## 7. CONCLUSIONS

Significant progress has been made in the characterization of the LII process, and in development of LII for single-shot time-and-space resolved quantitative measurement of particulate concentration

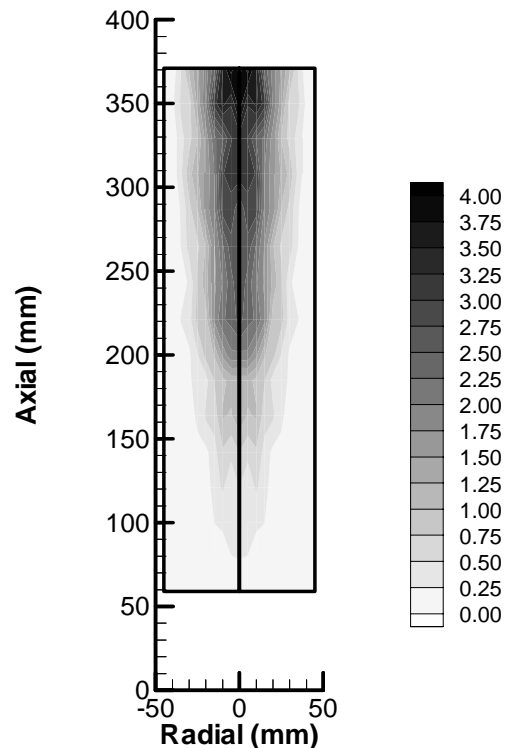


Figure 6 Distribution of time-averaged soot volume fraction (parts per billion) acquired by LII in a confined turbulent diffusion flame. Data at each grid location is the mean of 5000 single-shot measurements.

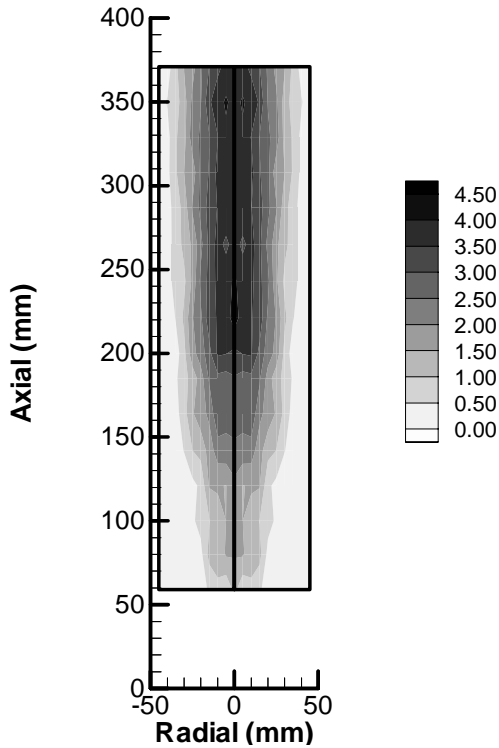


Figure 7 Probability (in percent) that measurable quantities of soot are present in the probe volume on a single-shot basis. Data acquired in a propane/air diffusion flame by LII.

in practical applications, such as turbulent combustion.

1. The LII signal has been shown to be proportional to soot volume fraction over the range 0.5 - 5 ppm.
2. Due to the large dynamic range of the LII technique we have been able to estimate soot concentrations in the 10 part per billion range while maintaining a spatial resolution of ~0.5 mm cubed. A further factor of ten increase in sensitivity could be obtained by relaxing the dimensions of the probe volume to a 1.0 mm cube.
3. The rate of decay of the LII signal in the post evaporative region (>300 ns after excitation) is shown to be a sensitive measure of particle size. For soot, the size measured appears to be the primary particle size rather than some average agglomerate size. While the numerical model was able to successfully predict post evaporative LII signal decay rates.
4. More work needs to be done before the currently available LII models can correctly predict the soot particle behaviour during soot evaporation.

5. The application of LII to measure soot volume fraction in a turbulent diffusion flame has been successfully demonstrated.

## 8. FUTURE WORK

It remains to be demonstrated that the LII signal is strictly proportional to soot volume fraction over several orders of magnitude change in soot concentration. Both our results and the original modelling of Melton<sup>6</sup> predict that the prompt LII signal will vary as the 3.33 power of particle diameter (for LII detection at 450 nm). This predicted departure from strict proportionality between LII signal and soot volume fraction has not been experimentally observed in this work or by others.

### Acknowledgements:

This work was supported in part by PERD Committee 1.5 of the Canadian Government, by the National Research Council's internal research funds, and by the Department of National Defence. We thank: Dan Gareau for his technical support in configuring the LII apparatus and the laminar burner, and in performing the experiments; Doug Logan for his technical support with the turbulent burner; and Dan Fetter for assistance in modeling and data analysis.

### Nomenclature:

$c$	- speed of light
$C_a$	- soot particle absorption cross section
$c_p$	- specific heat at constant pressure
$c_s$	- specific heat of carbon
$c_v$	- specific heat at constant volume
$D_{AB}$	- interdiffusion coefficient for soot vapour into surrounding gas
$D_{ES}$	- diameter of soot equivalent sphere
$d_p$	- diameter of soot primary particles
$f$	- Eucken factor
$G$	- geometry dependent heat transfer factor
$H_v$	- heat of vaporization
$K_a$	- thermal conductivity of ambient air
$K_{ap}$	- absorption efficiency (for primary particles)
$K_n$	- Knudsen number ( $K_n = \lambda_{MFP} / D_{ES}$ )
$M$	- mass of carbon
$M_V$	- molecular weight of carbon vapour
$M_A$	- molecular weight of air
$N_{av}$	- Avogadro's number
$N_P$	- number of primary particles in agglomerate
$P_S(T)$	- pressure of soot vapour
$q$	- laser fluence
$T$	- soot surface and vapour temperature
$T_0$	- gas temperature
$\alpha$	- accommodation coefficient
$\gamma$	- $c_p/c_v$
$\lambda$	- wavelength
$\lambda_{MFP}$	- mean free path

$\rho_s$	- density of soot
$\sigma_{SB}$	- Stefan-Boltzmann constant
$\tau$	- LII decay signal time constant
T	- light transmission through flame

## References

- R. A. Dobbins and C. M. Megaridis, "Morphology of flame-generated soot as determined by thermophoretic sampling," *Langmuir* **3**, 254-259 (1987).
- R. A. Dobbins and C. M. Megaridis, "Absorption and scattering of light by polydisperse aggregates," *Applied Optics* **30**, 4747-4754 (1991).
- U. O. Koylu and G. M. Faeth, "Optical properties of overfire soot in buoyant turbulent diffusion flames at long residence times," *Journal of Heat Transfer* **116**, 152-159 (1994).
- U. O. Koylu and G. M. Faeth, "Optical properties of soot in buoyant laminar diffusion flames," *Journal of Heat Transfer* **116**, 971-979 (1994).
- C. J. Dasch, "New soot diagnostics in flames based on laser vaporization of soot," 20th Symposium (International) on Combustion, , 1231-1237 (1984).
- L. A. Melton, "Soot diagnostics based on laser heating," *Applied Optics* **23**, 2201-8 (1984).
- J. E. Dec, A. O. zur Loye, and D. L. Siebers, "Soot distribution in a D.I. diesel engine using 2-D laser-induced incandescence imaging," *SAE Transactions* **100**, 277-288 (1991).
- R. L. Vander Wal and K. J. Weiland, "Laser-induced incandescence: Development and characterization towards a measurement of soot-volume fraction," *Applied Physics B* **59**, 445-452 (1994).
- R. Puri, T. F. Richardson, R. J. Santoro, and R. A. Dobbins, "Aerosol dynamic processes of soot aggregates in a laminar ethene diffusion flame," *Combustion and Flame* **92**, 320-333 (1993).
- D. L. Hofeldt, "Real-time soot concentration measurement technique for engine exhaust streams," SAE Paper No. 930079 (1993).
- P. E. Bengtsson and M. Alden, "Soot-visualization strategies using laser techniques: Laser-induced fluorescence in C2 from laser-vaporized soot and laser-induced soot incandescence," *Applied Physics B* **60**, 51-59 (1995).
- B. S. Mewes and J. M. Seitzman, "Soot volume fraction and particle size measurements with laser-induced incandescence," *Applied Optics* **36**, 709-717 (1997).
- N. P. Tait and D. A. Greenhalgh, "PLIF imaging of fuel fraction in practical devices and LII imaging of soot," *Berichte der Bunsengesellschaft fuer Physikalische Chemie* **97**, 1619-1625 (1993).
- S. Will, S. Schraml, and A. Leipertz, "Two-dimensional soot-particle sizing by time-resolved laser-induced incandescence," *Optics Letters* **20**, 2342-2344 (1995).
- Ö. L. Gülder, "Influence of hydrocarbon fuel structural constitution and flame temperature on soot formation in laminar diffusion flames," *Combustion and Flame* **78**, 179-194 (1989).
- W. H. Dalzell and A. F. Sarofim, "Optical constants of soot and their application to heat flux calculations," *Journal of Heat Transfer* **91**, 100-104 (1969).
- C. J. Dasch, "One-dimensional tomography: a comparison of Abel, onion-peeling, and filtered backprojection methods.," *Applied Optics* **31**, 1146-1152 (1992).
- R. A. Dobbins, R. J. Santoro, and H. G. Semerjian, "Analysis of light scattering from soot using optical cross sections for aggregates," 23rd Symposium (International) on Combustion , 1525-1532 (1990).
- G. M. Faeth and U. O. Koylu, "Soot morphology and optical properties in nonpremixed turbulent flame environments," *Combustion Science and Technology* **108**, 207-229 (1995).
- C. R. Shaddix and K. C. Smyth, "Laser induced incandescence measurements of soot production in flickering methane, propane, and ethylene diffusion flames," *Combustion and Flame* **107**, 418-452 (1994).
- T. P. Ni, J.A.; Gupta, S.; Santoro, R.J., "Two-dimensional imaging of soot volume fraction by the use of laser-induced incandescence," *Applied Optics* **34**, 7083-7091 (1995).
- B. Quay, T. W. Lee, T. Ni, and R. J. Santoro, "Spatially resolved measurements of soot volume fraction using laser-induced incandescence," *Combustion and Flame* **97**, 384-392 (1994).
- R. L. Vander Wal, Z. Zhou, and M. Y. Choi, "Laser-induced incandescence calibration via gravimetric sampling," *Combustion and Flame* **105**, 462-470 (1996).
- A. C. Eckbreth, T. J. Anderson, and G. M. Dobbs, "Conditional sampling for fuel and soot in CARS thermometry," 21st Symposium (International) on Combustion , 1747-1754 (1986).
- C. J. Dasch, "Continuous-wave probe laser investigation of laser vaporization of small soot particles in a flame," *Applied Optics* **23**, 2209-2215 (1984).
- B. J. McCoy and C. Y. Cha, "Transport phenomena in the rarefied gas transition regime," *Chemical Engineering Science* **29**, 381-388 (1974).
- H. R. Leider, O. H. Krikorian, and D. A. Young, "Thermodynamic properties of carbon up to the critical point," *Carbon* **11**, 555-563 (1973).
- C. M. Megaridis and R. A. Dobbins, "Comparison of soot growth and oxidation in smoking and non-smoking ethylene diffusion flames," *Combustion Science and Technology* **66**, 1-16 (1989).
- J. Appel, M. Jungfleisch, M. Marquardt, R. Suntz, and H. Bockhorn, "Assessment of soot volume fractions from laser-induced-incandescence by comparison with extinction measurements in

- laminar premixed flat flames," 26th Symposium (International) on Combustion , 2387-2395 (1996).
30. O. Leroy, J. Perrin, J. Jolly, and M. Pealat, "Thermal accommodation of a gas on a surface and heat transfer in CVD and PECVD experiments," Journal of Physics D 30, 499-509 (1997)